**Iğdır Üniversitesi Fen Bilimleri Enstitüsü Dergisi, 11(4): 2955-2966, 2021**
**Journal of the Institute of Science and Technology, 11(4): 2955-2966, 2021**

**ISSN: 2146-0574, eISSN: 2536-4618**

**Kimya / *Chemistry*** **DOI: 10.21597/jist.953803**

**Araştırma Makalesi / *Research Article***

**Geliş tarihi / Received: 17.06.2021** **Kabul tarihi / Accepted: 18.07.2021**

**Atıf İçin:** Tekeş AT, Ata AC, Tanrıverdi AA, Çakmak İ, 2021. THBF Bileşiğinin Insiliko Moleküler Yerleştirme Çalışmaları: TD-DFT Simülasyonları ve İlaç Tasarımı. Iğdır Üniversitesi Fen Bilimleri Enstitüsü Dergisi, 11(4): 2955-2966.

**To Cite:** Tekeş AT, Ata AC, Tanrıverdi AA, Cakmak İ, 2021. Insilico Molecular Docking Studies of THBF Compound: TD-DFT Simulations and Drug Design. Journal of the Institute of Science and Technology, 11(4): 2955-2966.

# THBF Bileşiğinin Insiliko Moleküler Yerleştirme Çalışmaları: TD-DFT Simülasyonları ve İlaç Tasarımı

Ahmet Turan TEKEŞ[1], Ahmet Cağrı ATA[1], Aslıhan Aycan TANRIVERDİ[1*], İsmail ÇAKMAK[1]

**ÖZET:** Bu çalışmada, 4 - ((2*R*, 3*S*) -2, 3, 4-trihidroksibutoksi) ftalonitrilin geometrik yapılarının B3LYP / 6-311G (d, p) ve elektronik özelliklerine dayalı detaylı bir TD-DFT çalışması sunuyoruz. Çalışma, enerji boşluğu (Δ), İyonlaşma potansiyeli (I), Elektron Afinitesi (A), Global Sertlik (η), Kimyasal Potansiyel (μ), Global Elektrofilik (ω), Elektronejisite (ε) hesaplamak için HOMO-LUMO analizine genişletildi. Hesaplanan HOMO ve LUMO enerjisi, molekül içinde meydana gelen yük transferlerini ortaya çıkarır. Sonuçlar grafikler, tablolar ve şekiller ile gösterildi. Bileşiğin doğrusal olmayan özellikleri belirlendi. Ligand-protein etkileşimlerinin tam bağlanma bölgesini ve bağlanma mekanizmasını araştırmak için moleküler yerleştirme sağlandı.

**Anahtar Kelimeler:** Ftalonitril, TD-DFT, HOMO-LUMO, moleküler yerleştirme, ilaç tasarımı

## *Insilico* Molecular Docking Studies of THBF Compound: TD-DFT Simulations and Drug Design

**ABSTRACT:** In this study, we present a detailed TD-DFT study based on the B3LYP / 6-311G (d, p) and electronic properties of geometric structures of 4 - ((2*R*, 3*S*) -2, 3, 4-trihydroxybutoxy) phthalonitrile. The study was expanded to HOMO-LUMO analysis to calculate energy gap (Δ), Ionization potential (I), Electron Affinity (A), Global Hardness (η), Chemical Potential (μ), Global Electrophilicity (ω), Electronegicity (ε). Calculated HOMO and LUMO energy reveal charge transfers that occur within the molecule. The results were shown with graphs, tables, and figures. Nonlinear properties of the compound have been determined. Molecular docking was achieved to probe the complete binding site and binding mechanism of the ligand-protein interactions.

**Keywords:** Phthalonitrile, TD-DFT, HOMO-LUMO, molecular docking, drug design

[1]Ahmet Turan TEKEŞ (**Orcid ID:** 0000-0002-9942-7367), Ahmet Çağrı ATA (**Orcid ID:** 0000-0002-2296-2265), Aslıhan Aycan TANRIVERDİ (**Orcid ID:** 0000-0001-5811-8253), İsmail ÇAKMAK (**Orcid ID:** 0000-0002-3191-7570), Kafkas Üniversitesi, Fen-Edebiyat Fakültesi, Kimya Bölümü, Kars, Türkiye

***Sorumlu Yazar/Corresponding Author:** Aslıhan Aycan TANRIVERDİ, e-mail: t.aslihanaycan@gmail.com

## INTRODUCTION

As a group of compounds, phthalocyanines (Pc) have been used widely in basic research and have been used widely employed in several sectors from industrial to technological fields. Information on different synthesis pathways and structures for phthalocyanines is well established (McKeown 1998; Zhang et al., 2010; George 2018; Ağırtaş et al., 2021). Over the past three decades, an increasingly strong correlation has emerged between PC features and applications (Leznoff et al., 1989; McKeown 1998; George 2018). Optical and light sensitivity properties (De La Torre et al., 2001; Isago 2015; Okura 2017), as well as paint and pigment grades (Gregory 2003), have always been at the forefront of PC research. Once the basics of synthesis and features were understood, new applications began to be explored, which could benefit from its extraordinary electronic properties and led to its use as materials and devices (Claessens et al., 2008). This led to the use of PCs in paint-sensitive solar cells (DSSC), which was recently extensively reviewed (Urbani et al., 2019). Recently, PCs have found applications in biological systems, especially photodynamic therapy (PDT) (Lo et al., 2020), nanobiotechnology and theranostics (Zafar et al., 2016).

We felt that an updated review of PCs was desirable in the field of new applications that have not yet been addressed. These areas include the use of PCs in chemical sensor technology, nonlinear optics (NLO), and energy storage applications. Many different studies have been conducted to theoretically investigate the electrical properties of the conjugate π system in phthalocial compounds (highest occupied molecular orbital (HOMO) and lowest unoccupied molecular orbital (LUMO), stimulation energies) (Zagal et al., 2010; Urbani et al., 2019; Cabir et al., 2020; Lo et al., 2020). Density functional theory (DFT) is known as the most widely used method, with results and rational phenomenon in modeling medium and large molecules (Yİldİko et al., 2021). However, HOMO and LUMO energies calculated by DFT and TD-DFT methods illuminate specific interactions as well as dielectric properties in the molecular system (CagriAta et al., 2021).

We felt that an updated review of PCs was desirable in the field of new applications that have not yet been addressed. These areas include the use of PCs in chemical sensor technology, nonlinear optics (NLO), and energy storage applications. Numerous studies have been carried out to theoretically examine the electronic structure of the conjugate π system of phthaloyl composites (Zagal et al., 2010; Cabir et al., 2019; Urbani et al., 2019; Lo et al., 2020;). Density functional theory (DFT) appropriately represents the preferred approach for modeling medium and large molecules with emerging results (Güngördü Solğun et al., 2019; Solğun et al., 2020; Ağırtaş et al., 2020; Solğun et al., 2021). However, HOMO and LUMO energies calculated using DFT and TD-DFT methods demonstrate dielectric characteristics and specific interactions in a molecule. Molecular docking was performed binding mechanism of the ligand-protein interactions.

## MATERIALS AND METHODS

### Computer Calculations

The THBF molecule was first drawn in ChemBioDraw for TD-DFT calculations in the gaussian 09 program and minimized by SYBL2 (mol2) method with Chem3D program. Similarly, the drawn molecules were converted to 3D MOL2 files in Chem3D and transferred to GaussView 6.0. TD-DFT study was calculated on 6-311G basis set in B3LYP and LanL2DZ method and images of each calculation (Geometry optimization, HOMO and LUMO analysis, Mulliken atomic charges and MEP analysis) were taken. Molecular docking was provided to investigate the exact binding site and binding mechanism of ligand-protein interactions. Schrödinger's Maestro Molecular Modeling platform (version 11.8). The LLC model was applied in the molecular docking approach. High resolution (1.55-2.10 A)

crystal structures of human glutathione S-transferase of subunit type 1 (hGSTA1-1) (PDB: 5JCU), human acetylcholinesterase (hAChE) (PDB: 6O4W) and butyrylcholinesterase (BChE) (PDB: 6SAM) enzymes were downloaded. All compounds were equiped as for that former studies with the Ligprep module. At the same time, all the water molecules in the crystalline structure were deleted individually. With this module, protein ion balance was regulated by designating the active site of the protein for flexible binding. Using the receptor grid module, grid boxes were created to let flexible docking by making grids on the protein's binding sites, as for that former studies (Wang et al., 2020). Ligand-protein docking studies were performed with the glide docking module. The highest binding energies and binding conformations between ligands and enzymes were estimated. The lowest energy positions show the highest binding affinities. The resulting receptor 3D interactions were visualized with Discovery Studio 2016 client (Visualizer 2005).

## RESULTS AND DISCUSSION

### TD-DFT Studies

### Geometry optimization

THBF optimized basic structure and total energy conversion are given in Figure 1. The 6-311G (d, p) basis set of TD-DFT-B3LPY and the optimized bond length parameters of the molecule calculated with LanL2DZ are listed in Table 1. Two optimized methods of the THBF compound were compared. This means that the structure has minimal potential energy. All connective lengths and connective angles in phenyl rings are within the normal range. The bond distances for C-C for B3LYP are 1,392-1,544 Å and 1,401-1,532 Å for LanL2DZ, and the 1,414 to 1,443 Å C-O bond distances for these values belong to the oxygen atom between the two phenyl rings. The lengths of C-H in the aromatic ring are 1,078 - 1,080 Å. All C-C-C angles range from 112° to 122°. The C-C-H angle in the compound is 106 ° -109 °, C-C-O is 104 ° -112 °, and O-C-H is 110-112 °. There are very small differences between the B3LYP and LanL2DZ values. Theoretically calculated values of some phthalonitrile compounds may give insight into the geometry of molecular changes.

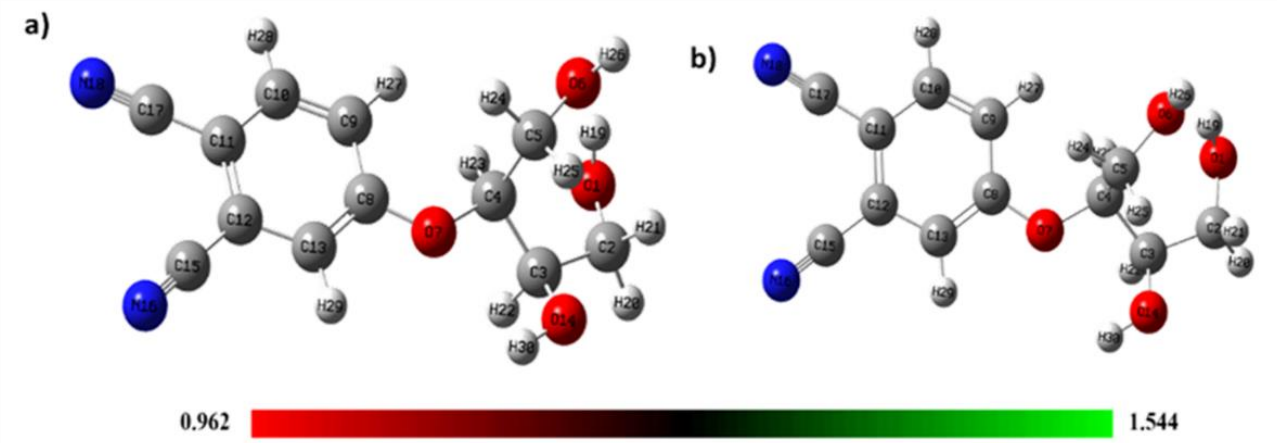


**Figure 1**. The structure of the THBF compound optimized using the TD-DFT method a) B3LYP/ 6-311G and b) LanL2DZ basis set.

**Table 1**. Theoretically obtained bond lengths (Å), connective angles (º), and dihedral angles (º) of the molecule

| Bond lengths (Å) | | | Bond angles (º) | | |
|---|---|---|---|---|---|
| **Atomic Groups** | **B3LYP** | **LanL2DZ** | **Atomic Groups** | **B3LYP** | **LanL2DZ** |
| O1-C2 | 1.414 | 1.443 | O1-C2-C3 | 112.8 | 111.7 |
| O1-H19 | 0.966 | 0.984 | C2-O1-H19 | 106.1 | 108.6 |
| C2-H21 | 1.095 | 1.097 | O1-C2-H21 | 112.1 | 111.9 |
| C2-H20 | 1.091 | 1.090 | O1-C2-H20 | 107.8 | 106.8 |
| C2-C3 | 1.538 | 1.535 | C2-C3-C4 | 112.7 | 112.0 |
| C3-O14 | 1.416 | 1.447 | H21-C2-H20 | 107.7 | 108.4 |
| C3-H22 | 1.097 | 1.098 | C3-C2-H21 | 108.1 | 108.2 |
| O14-H30 | 0.963 | 0.977 | C3-C2-H20 | 107.9 | 109.3 |
| C3-C4 | 1.544 | 1.532 | C2-C3-O14 | 106.5 | 105.9 |
| C4-H23 | 1.092 | 1.092 | C3-C4-O14 | 111.1 | 111.1 |
| C4-O7 | 1.443 | 1.471 | C3-O14-H30 | 108.3 | 110.9 |
| C4-C5 | 1.533 | 1.532 | H22-C3-O14 | 110.8 | 110.7 |
| C5-H24 | 1.095 | 1.095 | H22-C3-C2 | 109.3 | 110.3 |
| C5-H25 | 1.094 | 1.095 | H22-C3-C4 | 106.1 | 107.1 |
| C5-O6 | 1.429 | 1.458 | C3-C4-C5 | 114.7 | 114.4 |
| O6-H26 | 0.961 | 0.975 | C3-C4-H23 | 109.0 | 109.6 |
| C8-O7 | 1.349 | 1.363 | C4-C5-O6 | 106.8 | 106.8 |
| C8-C9 | 1.425 | 1.438 | C5-C4-O7 | 108.2 | 108.4 |
| C9-H27 | 1.078 | 1.080 | C5-C4-H23 | 109.7 | 109.9 |
| C9-C10 | 1.392 | 1.401 | C4-C5-H24 | 108.7 | 109.7 |
| C10-H28 | 1.082 | 1.084 | C4-C5-H25 | 109.2 | 109.9 |
| C10-C11 | 1.412 | 1.426 | H24-C5-H25 | 109.3 | 109.9 |
| C11-C12 | 1.459 | 1.455 | C5-O6-H26 | 109.0 | 112.3 |
| C12-C13 | 1.428 | 1.432 | H25-C5-O6 | 112.0 | 111.3 |
| C8-C13 | 1.405 | 1.414 | H24-C5-O6 | 110.5 | 109.9 |
| C13-H29 | 1.081 | 1.083 | O7-C4-C3 | 104.4 | 104.4 |
| C12-C15 | 1.394 | 1.408 | O7-C4-H23 | 110.2 | 109.9 |
| C15-N16 | 1.168 | 1.185 | C4-O7-C8 | 122.5 | 122.6 |
| C11-C17 | 1.407 | 1.419 | O7-C8-C13 | 113.9 | 114.3 |
| C17-N18 | 1.162 | 1.180 | O7-C8-C9 | 123.0 | 122.7 |
| **Dihedral Angles (º)** | | | | | |
| **Atomic Groups** | **B3LYP** | **LanL2DZ** | **Atomic Groups** | **B3LYP** | **LanL2DZ** |
| H19-O1-C2-C3 | 82.9 | 80.2 | H22-C3-C4-C5 | 179.8 | 64.0 |
| O1-C2-C3-H22 | 71.1 | 77.2 | C2-C3-C4-H23 | 63.2 | 58.8 |
| H20-C2-C3-O14 | 73.0 | 78.9 | O14-C3-C4-C5 | 59.1 | 60.5 |
| H21-C2-C3-C4 | 78.9 | 81.6 | H22-C3-C4-O7 | 61.3 | 69.6 |

## Frontier moleculer orbitaller (HOMO – LUMO)

The main electrical parameters related to orbitals in a molecule are the highest occupied molecular orbital (HOMO) and the lowest unoccupied molecular orbital (LUMO) and energy gaps. HOMO is the outermost (highest energy) orbital electrons that can function as an electron donor. LUMO is the innermost (lowest energy) orbit that has enough space to accept electrons and can function as an electron accent. HOMO and LUMO orbitals specify the interaction of the molecule with other types. The orbital representation of HOMO and LUMO for the density THBF molecule is shown in Figure 2. $E_{HOMO}$ -7.1850 eV - $E_{LUMO}$ -2.6997 eV for B3LYP method with TD-DFT method and $E_{HOMO}$ -8.6599 eV - $E_{LUMO}$ -1.5723 eV for LanL2DZ method were calculated. HOMO and LUMO orbitals regulate how the molecule interacts with other types. It also aids to characterize band space chemical reactivity and kinetic stability. A small boundary indicates the polarization, hardness, electronegativity, and other reactivity intakes of a molecule with an orbital gap. Table 2 shows the chemical reactivity indices.

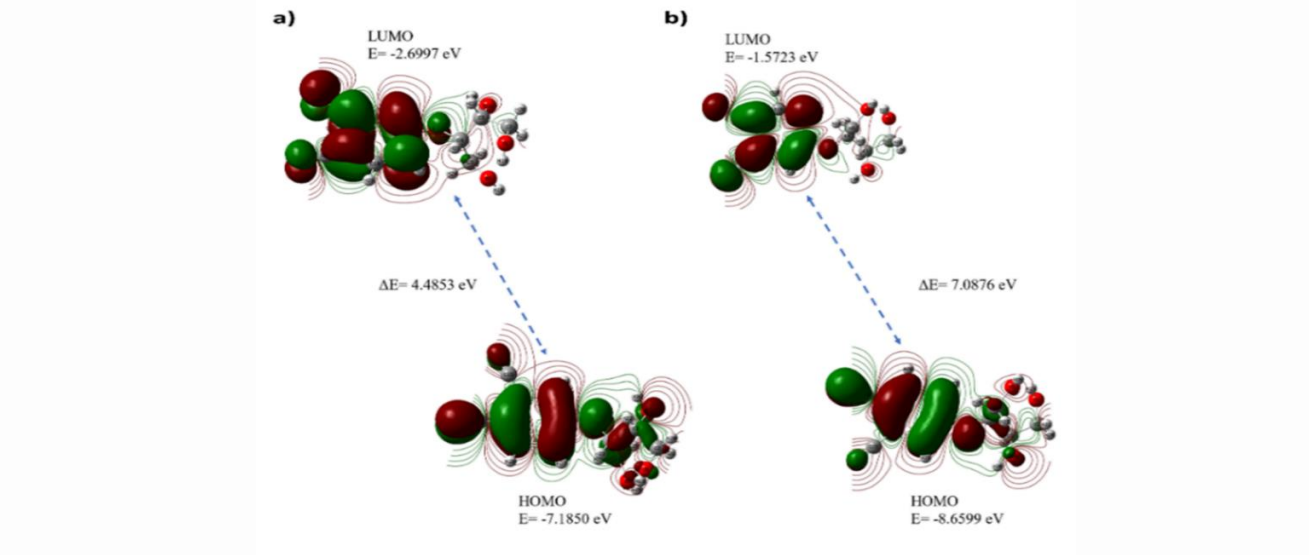


**Figure 2.** HOMO-LUMO energy maps and bandwidth using a) B3LYP andı b) LanL2DZ basis set by TD-DFT method for THBF molecule

**Table 2**. Comparison of molecular properties related to HOMO-LUMO energy cavities (D) and THBF molecule (au)

| **Molecular Energy** | **B3LYP** | **LanL2DZ** |
|---|---|---|
| $E_{LUMO}$ | -2.6997 | -1.5723 |
| $E_{HOMO}$ | -7.1850 | -8.6599 |
| $E_{LUMO+1}$ | -1.8447 | -0.6952 |
| $E_{HOMO-1}$ | -7.7075 | -9.2174 |
| Energy gaps (Δ) $\lvert E_{HOMO}- E_{LUMO}\rvert$ | 4.4853 | 7.0876 |
| Ionization Potential ($I = -E_{HOMO}$) | 7.1850 | 8.6599 |
| Electron affinity ($A = -E_{LUMO}$) | 2.6997 | 1.5723 |
| Chemical hardness ($\eta = (I - A)/2$) | 2.2426 | 3.5438 |
| Global Softness ($s = 1/2\ \eta$) | 1.1213 | 1.7719 |
| Chemical potential ($\mu = -(I + A)/2$) | -4.9423 | -5.1161 |
| Electronegativity ($\chi = (1+ A)/2$) | 1.8498 | 1.2861 |
| Global Electrophilicity ($\omega= \mu^2/2\ \eta$) | 5.4459 | 3.6929 |

**Molecular electrostatic potential surface (MEPS)**

Molecular electrostatic potential surface MEPS shows the shape size and electrostatic potential values of the molecule and are drawn for the phthalonitrile molecule. Molecular electrostatic potential (MEPS) mapping is very useful in investigating the physicochemical properties of molecular structure (Vanasundari et al., 2017). Some of the molecules with negative electrostatic potential are susceptible to electrophilic attack. The blue and red regions on the MEPS map answer to positive and negative potential regions and refer to electron-wealthy and electron-deficient regions respectively. The green color indicates neutral electrostatic potential.

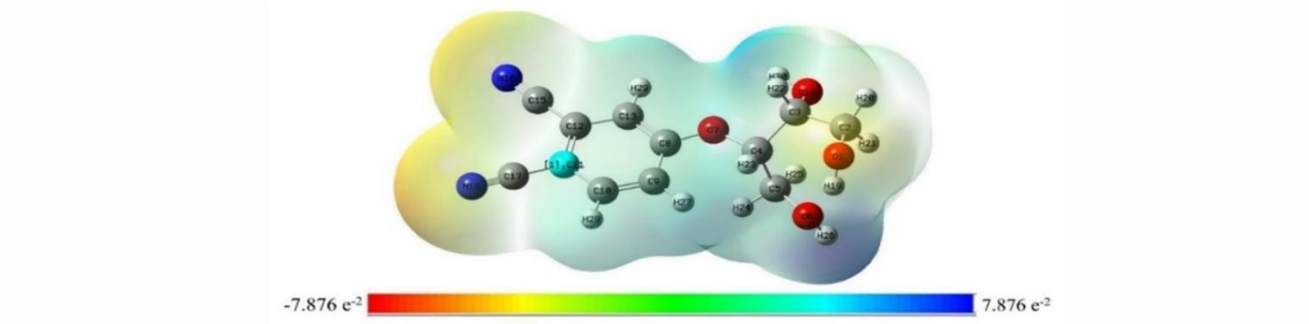


**Figure 3.** MEPS mapping of the THBF molecule

In this study molecular electrostatic potential (MEPS) maps were mapped for the THBF molecule. as displayed in Figure 3. In the case of phthalonitrile, the MEPS map shows the presence of negative potential regions around the nitrogen atoms which are characterized in red. A relatively larger region around the nitrogen atoms of the dibromo perylene molecule denotes the most negative potential region (dark red) and interaction is permitted. The hydrogen atom carries the maximum strength of the positive charge (dark blue). It shows an almost neutral potential as most of the aromatic ring region is represented by green.

**Mulliken atomic charges**

The calculation of mulliken atomic charges plays an important role in the application of quantum chemical calculations to the molecular system. Because atomic charges affect, molecular polarization, electronic structure and many features of molecular systems. The charge distribution indicates the formation of pairs of transmitters and receivers on the atom including charge transfer in the molecule. The mulliken atom was calculated in the basis set B3LYP / 6-311G (d. p) and LanL2DZ using the TD-DFT method. The data obtained are shown in Figure 4-5 and Table 3.

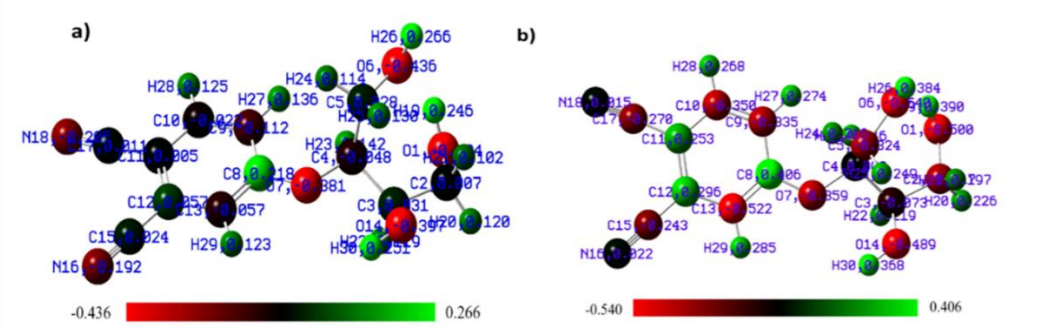


**Figure 4.** With the TD-DFT method of the THBF molecule a) B3LYP / 6-311G (d. p) and b) LanL2DZ basis set mulliken atomic charges

The distribution of the mulliken payload is that the oxygen atom attached to the aromatic ring is O1 (-0.403) - (-0.500). O6 (-0.435) - (-0.539). O7 (-0.381) - (-0.359). The charge value of the H atom connected to the aromatic ring has a positive charge. It was shown that while some C atoms were positive and some were negative.

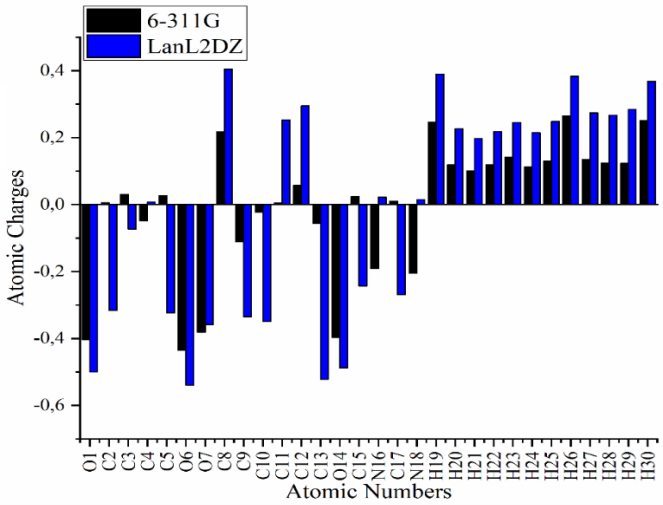


**Figure 5.** Comparison of mulliken atomic charges for the THBF molecule

**Table 3**. Mulliken atomic charges were calculated by the TD-DFT method with the basis set B3LYP / 6-311G (d. p) and LanL2DZ

| Atoms | 6-311G | LanL2DZ | Atoms | 6-311G | LanL2DZ |
|---|---|---|---|---|---|
| O1 | -0.403 | -0.500 | N16 | -0.191 | 0.022 |
| C2 | 0.006 | -0.316 | C17 | 0.010 | -0.269 |
| C3 | 0.031 | -0.073 | N18 | -0.205 | 0.015 |
| C4 | -0.048 | 0.008 | H19 | 0.246 | 0.390 |
| C5 | 0.027 | -0.323 | H20 | 0.119 | 0.226 |
| O6 | -0.435 | -0.539 | H21 | 0.101 | 0.197 |
| O7 | -0.381 | -0.359 | H22 | 0.119 | 0.218 |
| C8 | 0.217 | 0.405 | H23 | 0.142 | 0.245 |
| C9 | -0.111 | -0.335 | H24 | 0.113 | 0.215 |
| C10 | -0.022 | -0.349 | H25 | 0.129 | 0.248 |
| C11 | 0.005 | 0.253 | H26 | 0.265 | 0.383 |
| C12 | 0.057 | 0.295 | H27 | 0.135 | 0.274 |
| C13 | -0.056 | -0.522 | H28 | 0.124 | 0.267 |
| O14 | -0.397 | -0.488 | H29 | 0.123 | 0.285 |
| C15 | 0.024 | -0.243 | H30 | 0.251 | 0.368 |

**NBO analysis**

NBO analysis provides research on the most accurate Lewis structure of the molecule. the detailed electron density of all orbitals the NBO method is an assessment of full and empty orbital interactions that provide information about both inter-molecular and intermolecular interactions. In the NBO analysis of compound, a circumstantial Fock matrix was performed to evaluate transmitter-receiver interactions. The consequence of the interaction is a loss of occupancy from a localized NBO of the idealized Lewis structure to an empty non-Lewis orbit. For each transmitter (i) and receiver (j), the stabilization energy associated with the displacement of i → j is estimated as E (2). NBO analysis was performed to explain charge transfer or charge displacement due to intra-molecular interaction between the bonds. These results are delocalization and hyperconjugation measurements. The analyzed results are given in Table 4. Intra-molecular interactions are observed as an increase in electron density (ED) in antibody orbitals that weaken the relevant bonds (C - O). The occupancy rate of E bonds is higher than σ* ligaments which provides greater localization. The intra-molecular hyper conjugative interaction of the distribution to the electrons of the π π (C8-C9) in the ring (C8-C9) leads to the stabilization of part of the ring as shown in

Table 4. π* (C10-C11) and anti Ring * (C12-C13) lead to 25.61-18.56 kcal/mol stabilization. These values increased conjugation which led to strong localization.

**Table 4.** Selected NBO results for THBF molecule (TD-DFT) B3LYP / 6-311G (d. p) basis set)

| NBO(i) | Type | ED/e | NBO(j) | Type | ED//e | E(2)[a] (Kcal/mol) | E (j)-E(i)[b] (a.u.) | F (i. j)[c] (a.u) |
|---|---|---|---|---|---|---|---|---|
| O1-C2 | σ | 1.99381 | C3-O14 | σ* | 0.04747 | 1.31 | 1.11 | 0.034 |
| O1-H19 | σ | 1.98833 | C2-H20 | σ* | 0.02047 | 1.55 | 1.12 | 0.037 |
| C2-C3 | σ | 1.97792 | C3-C4 | σ* | 0.04747 | 0.72 | 0.96 | 0.024 |
| C2-H20 | σ | 1.98214 | O1-H19 | σ* | 0.01653 | 1.79 | 0.95 | 0.037 |
| C2-H21 | σ | 1.98703 | C3-O14 | σ* | 0.01999 | 1.09 | 0.80 | 0.026 |
| C3-C4 | σ | 1.97475 | C5-H24 | σ* | 0.02464 | 1.03 | 1.01 | 0.029 |
| C3-O14 | σ | 1.99086 | O1-C2 | σ* | 0.00791 | 1.50 | 1.15 | 0.037 |
| C3-H22 | σ | 1.97434 | C2-H21 | σ* | 0.02569 | 1.98 | 0.91 | 0.038 |
| C4-O7 | σ | 1.98612 | C2-C3 | σ* | 0.03846 | 1.39 | 1.21 | 0.037 |
| C4-H23 | σ | 1.97713 | C3-O14 | σ* | 0.01999 | 3.52 | 0.83 | 0.048 |
| C5-O6 | σ | 1.99151 | C4-O7 | σ* | 0.03349 | 2.07 | 1.09 | 0.043 |
| C5-H24 | σ | 1.98516 | C3-C4 | σ* | 0.04747 | 3.07 | 0.88 | 0.047 |
| O6-H26 | σ | 1.98875 | C4-C5 | σ* | 0.03155 | 2.10 | 1.08 | 0.043 |
| O7-C8 | σ | 1.99010 | C12-C13 | σ* | 0.02208 | 1.01 | 1.70 | 0.037 |
| C8-C9 | σ | 1.97976 | C8-C13 | σ* | 0.02054 | 4.03 | 1.24 | 0.063 |
| | π | 1.59934 | C10-C11 | π* | 0.38304 | 25.61 | 0.28 | 0.076 |
| | | | C12-C13 | π * | 0.37067 | 18.56 | 0.27 | 0.064 |
| C15-N16 | σ | 1.99344 | C12-C15 | σ* | 0.03019 | 10.02 | 1.58 | 0.113 |
| C17-N18 | σ | 1.99390 | C11-C17 | σ* | 0.03091 | 9.28 | 1.57 | 0.108 |

## Molecular Docking Studies

Molecular docking was achieved to probe the complete binding site and binding mechanism of the ligand-protein interactions. The Maestro Molecular Modeling platform (version 11.8) of the Schrödinger. LLC model was exerted in the molecular docking approach. High resolution (1.55-2.10 Å) crystal structures of human glutathione S-transferase of subunit type 1 (hGSTA1-1) (PDB: 5JCU). human acetylcholinesterase (hAChE) (PDB: 6O4W) and butyrylcholinesterase (BChE) (PDB: 6SAM) enzymes were downloaded (Wang et al., 2020). The molecular insertion method acts an important part in structure-basic drug design. It foresees the type of interaction and binding patterns between active site proteins and ligands as well as the interval and intimacy of the relevant functional groups. The option of the goal protein for docking withal the ligand is correlated to the binding energy value. The more negative the binding energy value of any species indicates. the better the ability to docking to target the protein. In this study, molecular docking analysis was achieved by ligand (Arivazhagan et al., 2021). Glucosinolate precursors in many eatable vegetables are effective in preventing cancer in chemically stimulated and transgenic gnawing models. Here. we record the crystal structures of the alpha class GST of subunit type 1 (hGSTA1) within a complex with the THBF plugin (Kumari et al., 2016). Structural studies of the catalytic subunit of acetylcholinesterase (AChE) developed after the amino acid sequence has been subtracted from cDNA cloning less than 20% of the AChE structures are therapeutically relevant human AChE (hAChE) target structures. With the help of Structure. design of new pharmacologically active molecule endures at least in part on the functionally topical accuracy of macromolecular structures for model basic drug design. In this article, we describe the development and properties of hAChE crystals of THBF and a new unit cell suitable for X-ray diffraction studies at room temperature. The succeeded solution of the room temperature 3.2 Å resolution structure of the hAChE complex enables us to examine the room temperature structures of fallen affinity complexes such as hAChE-dependent oxime reactivators. Where there may be conformational variation associated with

temperature. Under conditions approaching physiological temperature. awaited in both oxime and hAChE. it can lead to a more conscious structure-basic design (Gerlits et al., 2019). Alzheimer's disease (AD) is a neurodegenerative brain sickness with amyloid b peptide (Ab) accumulations (amyloid plaques) and oxidative stress products that contribute to the pathogenesis of the disease. Compounds that can interact with a singlet or multi goals included in AD pathogenesis are probable anti-Alzheimer's agents. Neurodegeneration and synaptic dysfunction in AD staidly effect the cholinergic system and reason a reduce in the levels of the neurotransmitter acetylcholine (ACh) which then products memory lapse and cognitive impairment that is particular for patients with AD. Butyrylcholinesterase (BChE) is cholinesterase (ChE) that enders cholinergic neurotransmission by catalyzing the hydrolysis of ACh. Inhibition of ACh hydrolysis in the brain is used to raise ACh levels and hereby restore cognitive function and alleviate AD symptoms. In the study, we are investigating the interaction of THBF's BchE crystals in AD (Košak et al., 2020).

In pursuit of electing the best pose in all ligand-enzyme docking. the binding modes were examined to comprehend their inhibition mechanisms. Fig. 6 shows the interaction of 3D and 2D as a result of the THBF-hGSTA1-1 docking study. The docking score in binding affinity with THBF-hGSTA1-1 was calculated as -6.690 cal/mol. Here the binding mechanism, ARG D:13 (1.92 Å). ILE D:106 (2.34 Å), LEU D:107 (3.02 Å) and GLY D:14 (2.27 Å) Conventional hydrogen bond bonded to the hydroxyl groups. LEU D:107 (4.59 Å) Pi-Alkyl bonded to the phenyl center. SER D:18 (2.35 Å) Conventional hydrogen bond bonded to the nitrile group. LEU D:163 (2.78 Å) Van der Waals bonded to the nitrile group is an example. In Fig. 7 3D and 2D interactions are given as a result of the THBF-hAChE docking study.

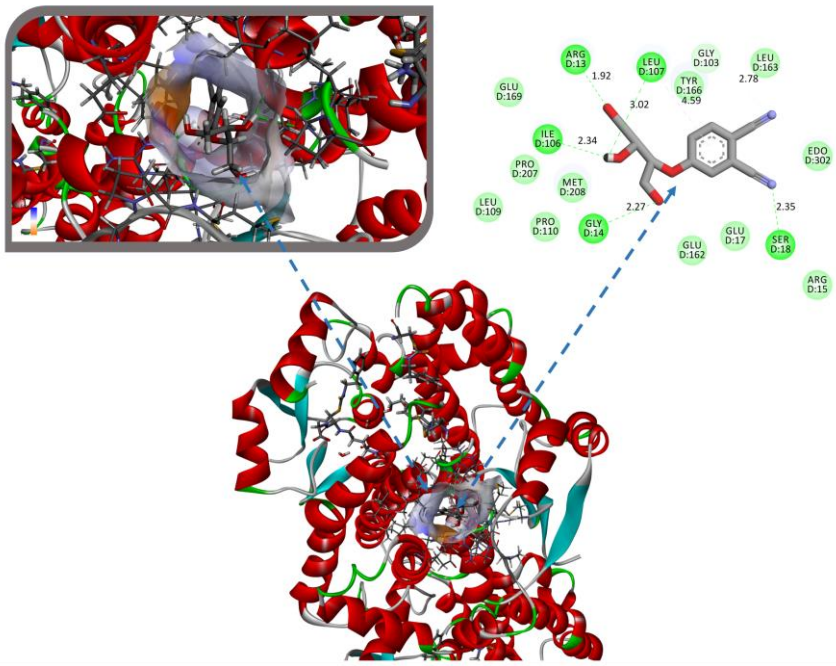


**Figure 6.** The interaction model between THBF – hGSTA1-1

The docking score in binding affinity with THBF-hAChE was calculated as -5.884 cal/mol. Here the binding mechanism. HOH A:729 (2.93 Å) Water hydrogen bond bonded to the hydroxyl group. TYR A:124 (2.32 Å). SER A:125 (2.85 Å). ASP A:74 (2.29 Å) and TYR A:337 (2.35 Å) Conventional hydrogen bond bonded to the hydroxyl groups. TRP A:86 (2.90 Å) Carbon hydrogen bond bonded to the hydroxyl group.

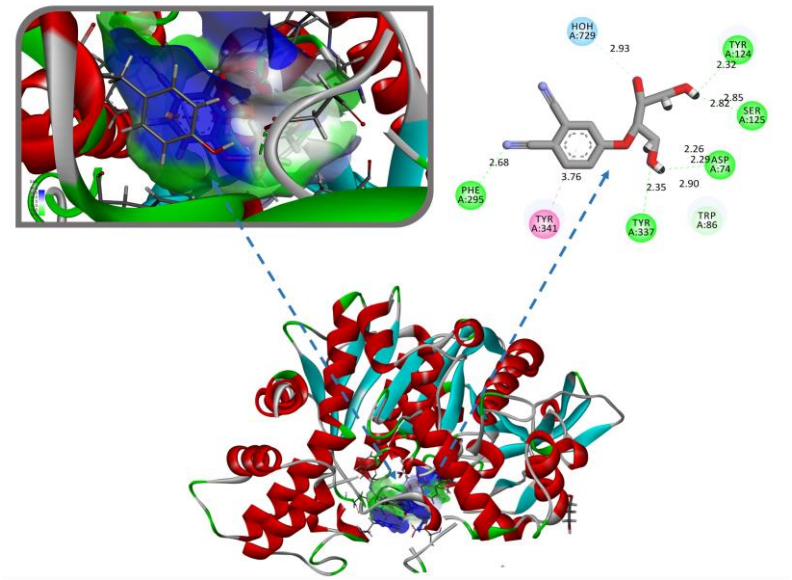


**Figure 7.** The interaction model between THBF – hAChE

TYR A:341 (3.76 Å) Pi-pi stacked bonded to the phenyl center. PHE A:295 (2.68 Å) Conventional hydrogen bond bonded to the nitrile group that are examples. The other interactions are in Figs. In Fig. 8 3D and 2D interactions are given as a result of the THBF-BChE docking study. The glide score in binding affinity with THBF-BChE was calculated as -4.834 cal/mol. Here the binding mechanism. ASP A:70 (2.05 Å) and HIS A:438 (2.13 Å) Conventional hydrogen bond bonded to the hydroxyl groups. SER A:198 (2.70 Å) and GLY A:117 (2.82 Å) Conventional hydrogen bond bonded to the hydroxyl groups bonded to the nitrile group that are examples. As a result of the research, the receptor molecules examined by molecular docking analysis were specified and it has emerged that THBF-hGSTA1-1 was more effective with the receptor binding score.

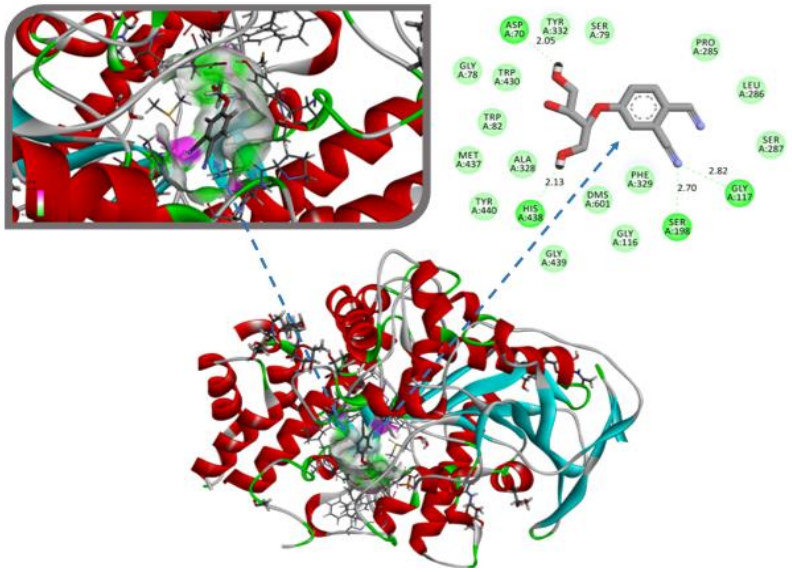


**Figure 8.** The interaction model between THBF – BChE

## CONCLUSION

In this study, theorical studies of 4 - ((2*R*, 3*S*) -2. 3. 4-trihydroxybutoxy) phthalonitrile compound were performed. Detailed research was carried out using quantum chemical calculations for the THBF molecule structural, electronic vibration frequencies of the compound were calculated by the TD-DFT

method with the basis set of B3LPY / 6-311G (d. p) and LanL2DZ. Structural parameters (bond lengths. bond angles and dihedral angles) were theoretically determined. Nonlinear optical properties were investigated. Finally, it was concluded that the compound examined could be used as a nonlinear optical (NLO) material as well as MEPS. HOMO-LUMO maps and mulliken while visualized charges are visualized available as a good intermediate material for synthesis. Thus taking into account this data for future synthesis studies minimizing the chemical consumption of molecules to be synthesized in the future and making the necessary predictions will provide significant conveniences for the synthesis of molecules. As a result of molecular docking studies, the receptor molecules were examined and it has emerged that THBF-hGSTA1-1 was more effective with the receptor glide score.

## ACKNOWLEDGEMENTS

For his support, Dr. We owe a great debt of gratitude to Ümit YILDIKO.

## Conflict of Interest

We declare that there is no a conflict of interest with any person, institute, company, etc.

## Author's Contributions

A.T.T., A.Ç.A, A.A.T., and İ.Ç. designed the study. A.T.T., A.Ç.A., A.A.T. performed the theoretical calculations. A.T.T., A.Ç.A, A.A.T., and İ.Ç. co-wrote the manuscript. All authors discussed the results and commented on the manuscript. All authors have given approval to the final version of the manuscript.

## REFERENCES

Ağırtaş MS, Cabir B, Gonca S and Ozdemir S, 2021. Antioxidant, Antimicrobial, DNA Cleavage, Fluorescence Properties and Synthesis of 4-(3, 4, 5-Trimethoxybenzyloxy) Phenoxy) Substituted Zinc Phthalocyanine. Polycyclic Aromatic Compounds, 1-15.

Ağirtaş MS, Solğun DG, Yildiko Ü, Özkartal A, 2020. Design of novel substituted phthalocyanines; synthesis and fluorescence, DFT, photovoltaic properties. Turkish Journal of Chemistry, 44 (6):1574-1586.

Arivazhagan R, Sridevi C, Prakasam A, 2021. Exploring molecular structure, spectral features, electronic properties and molecular docking of a novel biologically active heterocyclic compound 4-phenylthiosemicarbazide. Journal of Molecular Structure, 1232: 129956.

Cabir B, Yildiko U, Ağirtaş MS, 2019. Synthesis, DFT analysis, and electronic properties of new phthalocyanines bearing ETAEO substituents on peripheral position. Journal of Coordination Chemistry, 72 (17):2997-3011.

Cabir B, Yildiko U, Ağırtaş MS, Horoz S, 2020. Computational DFT calculations, photovoltaic properties and synthesis of (2R, 3S)-2, 3, 4-trihydroxybutoxy substituted phthalocyanines. Inorganic and Nano-Metal Chemistry, 50 (9):816-827.

CagriAta A, Yildiko Ü, Cakmak İ, Tanriverdi AA, 2021. Synthesis and characterization of polyvinyl alcohol-g-polystyrene copolymers via MADIX polymerization technique. Iranian Polymer Journal. 10.1007/s13726-021-00940-x.

Claessens CG, Hahn U and Torres T, 2008. Phthalocyanines: From outstanding electronic properties to emerging applications. The Chemical Record, 8 (2):75-97.

De La Torre G, Nicolau M, Torres T, 2001. In Supramolecular photosensitive and electroactive materials. Elsevier, pp. 1-111.

George L, 2018. Light-Activated Antimicrobial Materials Based on Perylene Imides and Phthalocyanines. http://urn.fi/URN:ISBN:978-952-15-4159-9.

Gerlits O, Ho K-Y, Cheng X, Blumenthal D, Taylor P, Kovalevsky A, Radić Z, 2019. A new crystal form of human acetylcholinesterase for exploratory room-temperature crystallography studies. Chemico-Biological Interactions, 309: 108698.

Gregory P, 2003. Metal complexes as speciality dyes and pigments.

Güngördü Solğun D, Salihağırtaş M and Yildiko U, 2019. Synthesis and structural characterization of HMBOS; A comparative MP2 and DFT study.10.13140/RG.2.2.25747.22566.

Isago H, 2015. Optical spectra of phthalocyanines and related compounds. Springer, pp. 21-40.

Košak U, Strašek N, Knez D, Jukič M, Žakelj S, Zahirović A, Pišlar A, Brazzolotto X, Nachon F, Kos J, Gobec S, 2020. N-alkylpiperidine carbamates as potential anti-Alzheimer's agents. European Journal of Medicinal Chemistry, 197: 112282.

Kumari V, Dyba MA, Holland RJ, Liang Y-H, Singh SV, Ji X, 2016. Irreversible Inhibition of Glutathione S-Transferase by Phenethyl Isothiocyanate (PEITC), a Dietary Cancer Chemopreventive Phytochemical. PLOS ONE, 11 (9):e0163821.

Leznoff C, Lever A, Properties and Applications, (VCH, New York, 1989).

Lo P-C, Rodríguez-Morgade MS, Pandey RK, Ng DK, Torres T, Dumoulin F, 2020. The unique features and promises of phthalocyanines as advanced photosensitisers for photodynamic therapy of cancer. Chemical Society Reviews, 49 (4):1041-1056.

McKeown NB, 1998. Phthalocyanine materials: synthesis, structure and function. Cambridge university press.

Okura I, 2017. Photosensitization of porphyrins and phthalocyanines. CRC Press.

Solğun D, Yıldıko Ü, Ağırtaş M, 2021. Synthesis, DFT calculations, photophysical, photochemical properties of peripherally metallophthalocyanines bearing (2-(benzo [d][1, 3] dioxol-5-ylmethoxy) phenoxy) substituents. Polycyclic Aromatic Compounds, 1-19.

Solğun DG, Keskin MS and Ağırtaş MS, 2020. DFT analysis and electronic properties, and synthesis of tetra (9-phenyl-9H-xanthen-9-yl) oxy peripheral-substituted zinc phthalocyanine. Chemical Papers, 1-13.

Urbani M, de la Torre G, Nazeeruddin MK, Torres T, 2019. Phthalocyanines and porphyrinoid analogues as hole- and electron-transporting materials for perovskite solar cells. Chemical Society Reviews, 48 (10):2738-2766.

Urbani M, Ragoussi M-E, Nazeeruddin MK, Torres T, 2019. Phthalocyanines for dye-sensitized solar cells. Coordination Chemistry Reviews, 381: 1-64.

Vanasundari K, Balachandran V, Kavimani M and Narayana B, 2017. Spectroscopic investigation, vibrational assignments, Fukui functions, HOMO-LUMO, MEP and molecular docking evaluation of 4–[(3, 4–dichlorophenyl) amino] 2–methylidene 4–oxo butanoic acid by DFT method. Journal of Molecular Structure, 1147: 136-147.

Wang G, Liu W, Gong Z, Huang Y, Li Y and Peng Z, 2020. Design, synthesis, biological evaluation and molecular docking studies of new chalcone derivatives containing diaryl ether moiety as potential anticancer agents and tubulin polymerization inhibitors. Bioorganic Chemistry, 95: 103565.

Yildiko Ü, Ata AÇ, Tanriverdİ AA and Çakmak İ, 2021. Investigation of novel diethanolamine dithiocarbamate agent for RAFT polymerization: DFT computational study of the oligomer molecules. Bulletin of Materials Science, 44 (3):186.

Zafar I, Arfan M, Nasir R, Shaikh A, 2016. Aluminum phthalocyanine derivatives: potential in antimicrobial PDT and photodiagnosis. Austin Biomolecules: Open Access, 1 (2):1-7.

Zagal JH, Griveau S, Silva JF, Nyokong T, Bedioui F, 2010. Metallophthalocyanine-based molecular materials as catalysts for electrochemical reactions. Coordination Chemistry Reviews, 254 (23-24):2755-2791.

Zhang Y, Cai X, Bian Y, Jiang J, 2010. Organic semiconductors of phthalocyanine compounds for field effect transistors (FETs). Functional Phthalocyanine Molecular Materials, 275-321.